Bimetallic CuFe nanoparticles as active and stable catalyst for chemoselective hydrogenation of biomass derived platform molecules

Karen S. Arias,† Lichen Liu,† Andrea Garcia-Ortiz, Maria J. Climent, Patricia Concepcion, Sara Iborra*, Avelino Corma*

Instituto de Tecnología Química, Universidad Politécnica de Valencia-Consejo Superior de Investigaciones Científicas (UPV-CSIC), Av. de los Naranjos s/n, 46022 Valencia, Spain

† These authors contribute equally to this work.

*Corresponding authors. E-mail: acorma@itq.upv.es (A.C.) siborra@itq.upv.es (S.I.)

Abstract

Bimetallic CuFe nanoparticles covered by thin carbon layers were developed as potential substitute for noble metal catalysts and have been used for chemoselective hydrogenation of 5-(hydroxymethyl)furfural (HMF) to 2,5-bis(hydroxymethyl)furan (BHMF). Compared to Cu catalysts supported on conventional solid carriers prepared by impregnation, the CuFe@C nanoparticles are active and more stable catalyst. The spatial distribution of the immiscible Cu and Fe in the bimetallic CuFe@C nanoparticles is dependent on the Cu/Fe ratio and moreover, an optimized Cu/Fe ratio has been found for hydrogenation of HMF. In the fresh Fe@C and CuFe@C catalysts, their surfaces are passivate and covered by FeOx, due to oxidation by air. Based on detailed structural characterizations and catalytic studies, small Cu nanoparticles supported on Fe nanoparticles are proposed to be the key active sites for hydrogenation of HMF. Those Cu nanoparticles can not only serve as the active sites for hydrogenation of HMF but also promote the reduction of FeOx into metallic Fe, resulting in an increased number of active sites in the bimetallic CuFe@C catalyst compared to monometallic Cu@C and Fe@C sample, resulting in a significant promotion of the catalytic activity.

Introduction

Biomass is considered as a renewable source and feedstock for production of fuels and chemicals in order to alleviate the society's dependence on fossil fuels. Platform molecules derived from biomass constitutes valuable starting compounds to obtain biofuels and high value-added chemicals.[1-3]

Furanic aldehydes such as furfural and 5-hydroxymethyl furfural (HMF), which can be obtained from non-edible lignocellulosic biomass, are versatile platform molecules that can be converted into a wide variety of important chemicals through numerous transformations.[4, 5]

Among them, hydrogenation of the carbonyl group of HMF to produce 2,5-bis(hydroxymethyl)furan (BHMF) has been intensively studied, since BHMF find numerous applications as intermediate in pharmaceuticals, as building block in polymeric materials and as biofuel additives.[6-8]

The hydrogenation of carbonyl group in biomass-derived platform molecules plays a key role for their catalytic transformation to fuels and chemicals.[3, 9, 10] The applications of metal catalysts based on noble metals (such as Pt, Pd, Ir, Ru etc) for the hydrogenation of furfural or HMF to corresponding alcohols or to the hydrodeoxygenation products have already been intensively studied[11-23]. Indeed, it has been shown in various works that, the introduction of a second metal (in most of the cases, a non-noble metal) can efficiently modulate the activity or selectivity of the noble metals.[24]

In recent years, the development of non-noble metal as substitutes for noble metal catalysts has attracted great attention in the catalysis community. Within this direction, it has been shown that non-noble metal nanoparticles (Ni, Fe, Co etc.) can exhibit high activity for the chemoselective hydrogenation of nitroarenes and excellent chemoselectivity to the corresponding anilines.[5, 25-28] Furthermore, the reactivity and selectivity of non-noble metal nanoparticles can be modulated either by introducing a second metal to form alloy nanoparticles or by introducing metal oxide as a second component for bifunctional catalyst.[29-34]

Considering the intrinsic properties of the non-noble metal elements, the miscibility between two metals can vary from miscible to immiscible, resulting in the formation of bimetallic nanoparticles with different distributions of the two elements within the metal particles. For instance, as shown in our previous work,[29] CoNi alloy nanoparticles can be prepared in a wide range of Co/Ni ratio and remain stable under reaction conditions. However, in the case of Cu and Fe, the formation of CuFe alloy phase is thermodynamically hindered (only 2.7 % of Cu in Fe phase at 850 ^{o}C according to the

phase diagram).[35] Therefore, these two elements usually remain in separated particles when supported on solid carriers, though the presence of both metals can be essential for desired catalytic performance, as observed in various catalytic systems.[36, 37] From a structural point of view, the geometric structure of CuFe bimetallic particles can be modulated by tuning the Cu/Fe ratio.[38] According to theoretical modelling, both core-shell and Janus structures can be present. In both cases, the interface between Cu and Fe will appear, in where the electronic structure of the metal will be modified and this may influence their catalytic behavior.

The preparation of CuFe bimetallic catalysts in the literature usually starts from inorganic precursors of Cu and Fe salts, followed by a reduction treatment. In those cases, the CuFe nanoparticles are not stable in contact with air and post-reduction temperatures at T >250 ºC is usually required. Recent works have reported that the hydrogenation of HMF to BHMF can be achieved with Cu-based metal.[39] However, the catalytic performances of the reported catalysts are still low and their stability is not always satisfying.[40, 41]

In this work, we will show a facile synthesis procedure for the preparation of stable CuFe bimetallic nanoparticles from the reduction of a very inexpensive organometallic CuFe complex, leading to the formation of bimetallic CuFe nanoparticles covered by thin carbon layers (CuFe@C nanoparticles). It has been found that Cu and Fe can work synergistically and when optimized, the bimetallic CuFe@C nanoparticles show excellent activity and high chemoselectivity for the hydrogenation of 5-(hydroxymethyl)furfural (HMF) into 2,5-bis(hydroxymethyl)furan (BHMF).

Results and Discussions

According to our previous works [5, 29, 30, 42, 43], the Fe@C nanoparticles were prepared by reducing the Fe-EDTA complex with H_2 at 450 ºC. As shown in **Figure 1a-b** and **Figure S1**, monodispersed metallic Fe nanoparticles with a metallic core and FeOx patches covered by thin carbon layers were obtained. When the Fe@C sample was tested for hydrogenation of 5-(hydroxymethyl)furfural (HMF) to 2,5-Bis(hydroxymethyl)furan (BHMF) under mild reaction conditions (110 ºC, 10 bar of H_2), a low activity was observed (see **Figure 2b**), probably due to the formation of surface FeOx patches from the irreversible re-oxidation by air. Those FeOx patches cannot be reduced under the reaction conditions, resulting in the blockage of the active metallic Fe sites. We have attempted to reduce the

Fe@C sample by H_2 at higher temperature (260 ºC, 6 h with 10 bar of H_2 in an autoclave, see **Figure S2**) prior to the catalytic test. The pre-reduced Fe@C sample shows similar performance as the pristine Fe@C sample for hydrogenation of HMF, indicating the difficulty to reduce the FeOx patches.

As reported in the literature, supported Cu catalysts are widely used for hydrogenation of biomass-derived carbonyl compounds.[40, 41] Besides, the addition of a proper amount of Cu catalysts can promoted the reactivity of Fe-based catalysts for CO/CO_2 hydrogenation reaction.[44] Inspired by those previous works, we have attempted first to load Cu on Fe@C nanoparticles to synthesize CuFe bimetallic catalysts for hydrogenation of HMF. By wetness impregnation, we have prepared a Cu/Fe@C sample with a Cu loading of ~25 wt% (named as 25Cu/Fe@C). As shown in **Figure 1c-f** and **Figure S3-S4**, Cu nanoparticles as well as highly dispersed Cu species are formed in the Cu/Fe@C sample, according to the X-ray energy dispersive spectroscopy (EDS) mapping results. Interestingly, the reactivity of the Cu/Fe@C sample is much higher than the pristine Fe@C, suggesting the significant promotion effect of Cu. Furthermore, to show the potential advantage of Fe@C nanoparticles as the support, we have prepared a series of supported catalysts with ~25 wt% Cu on conventional solid carriers by wetness impregnation, such as TiO_2, Al_2O_3, ZrO_2 and Fe_2O_3 (the resultant catalysts are named as 25Cu/support). The morphological characterizations on the distribution of Cu species on these samples are presented in **Figure S5 to S16**. Due to the high Cu loading, both highly dispersed Cu species and Cu nanoparticles are formed on the supports. Their catalytic performance for hydrogenation of HMF has been tested under the same conditions as 25Cu/Fe@C sample (see **Figure S17** for detailed catalytic results) and the yields of BHMF after 2 h of reaction (as summarized in **Figure 2c**) show that the 25Cu/Fe@C gives a better performance than the other Cu catalysts prepared with conventional supports.

Due to the presence of multiple types of Cu species (from big nanoparticles of >20 nm to subnanometric Cu clusters) in the 25Cu/Fe@C sample, it is difficult to determine the active sites and the activity per surface atom of Cu in this catalyst. Therefore, we have prepared a Cu/Fe@C sample with 5 wt% of Cu (named as 5Cu/Fe@C) to get a catalyst with more uniform Cu particle size. As shown in **Figure S18 to S20**, the vast majority of Cu species in the 5Cu/Fe@C sample are highly dispersed Cu species and only a few Cu nanoparticles can be observed in several areas. The catalytic results indicate that, the 5Cu/Fe@C sample is also active and selective for hydrogenation of HMF to

BHMF, though the activity is lower than the 25Cu/Fe@C sample when using the same amount of solid catalyst (see **Figure 2d**). However, if the initial reaction rate is normalized to the total amount of Cu (the Fe@C nanoparticles give negligible activity in the first few hours), the 5Cu/Fe@C sample is ~3.5-fold more active than the 25Cu/Fe@C sample (see **Figure 2e**), implying that highly dispersed Cu species on Fe@C nanoparticles could be the active sites for hydrogenation of HMF to BHMF.

Though the Cu/Fe@C samples are active and selective for hydrogenation of HMF to BHMF, a key parameter to be tested is their stability under reaction conditions. The leaching of Cu into the solvent is a common problem for supported Cu catalysts in catalytic applications related to biomass transformation. The metal leaching may cause the catalyst's deactivation, and the metal contamination in the liquids introduces challenges for the downstream processes.[45-47] When using 25Cu/Fe@C for hydrogenation of HMF, we have detected that ~10% of the Cu species were leached into the solvent and, indeed, the reused 25Cu/Fe@C catalyst showed a much lower activity in the second catalytic run (see **Figure S21**).

To prevent the metal leaching and structural transformation of supported metal catalysts in liquid-phase catalytic processes, coating the metal particles with thin layers of metal oxides or carbon materials has been reported as an effective strategy.[48, 49] In our previous work, we have demonstrated that, bimetallic CoNi nanoparticles can be generated within the coverage by thin carbon layers.[29] Therefore, we have attempted to prepare bimetallic CuFe nanoparticles, which are protected by thin carbon layers. In this context, the formation of bimetallic nanoparticles may enhance the interaction between Cu and Fe to form more active sites to catalyze the hydrogenation reaction, while the presence of thin carbon layers can protect the metallic nanoparticles from deep oxidation by air and the leaching in liquid-phase catalytic reactions.

Similar to the synthesis of Fe@C nanoparticles, the bimetallic CuFe@C nanoparticles were prepared by reducing the CuFe-EDTA complex with H_2 at 450 ^{o}C (see **Table S1** for the chemical compositions of various CuFe@C samples). The obtained CuFe@C nanoparticles (NPs) with different chemical compositions were firstly characterized by powder X-ray diffraction. As shown in **Figure 3**, only metallic Fe or metallic Cu can be observed in all the samples. For bimetallic CuFe@C samples, two separated diffraction patterns corresponding to Fe and Cu are observed. The intensities of the diffraction peaks corresponding to Fe and Cu vary with the chemical compositions of the bimetallic

CuFe samples accordingly, indicating the immiscible nature of the two metals.

The morphology of the non-noble metal nanoparticles was studied by field-emission scanning electron microscopy (FESEM). In the case of Cu@C sample, Cu NPs of 50-500 nm with a wider size distribution were observed (see **Figure 4a** and **Figure S22**). For bimetallic CuFe@C samples ($Cu_{0.75}Fe_{0.25}$, $Cu_{0.50}Fe_{0.50}$, $Cu_{0.24}Fe_{0.76}$, $Cu_{0.12}Fe_{0.88}$ and $Cu_{0.08}Fe_{0.92}$), isolated Cu@C and Fe@C nanoparticles, together with a mixture of Cu domains and Fe domains can be observed according to the FESEM-EDS mapping (see **Figure S23-S27**), indicating the complexity of the distributions of Fe and Cu in those samples. It should be noted that, either in Fe-dominant areas or in Cu-dominant areas, the overlapping of the two elements is confirmed. The bimetallic CuFe@C nanoparticles with different chemical compositions have also been studied by high-resolution TEM. As shown in **Figure S28-S37**, thin carbon layers and metal oxide patches are found in all the samples. The core of the nanoparticles remains to be metallic, being consistent with the XRD patterns.

Taking a careful look at the HRTEM images on various samples, it seems that, the metallic state of Cu in the Cu@C sample is more preserved than metallic Fe phase in Fe@C sample after the contact with air, since the presence of CuOx patches is barely observed in the HRTEM images (see **Figure S38**). Such difference can be explained by the distinct stability of metallic Cu and Fe in air. Metallic Fe will be rapidly oxidized by air at room temperature, giving to the formation of FeOx patches on the nanoparticle surface while the metallic Cu is much more stable.

To obtain more detailed information on the spatial distributions of Cu and Fe in the bimetallic CuFe samples, we have carried out STEM-EDS analysis, which offers a higher resolution for the comparison between different samples. As shown in **Figure S39**, a large number of Cu nanoparticles as well as some Fe nanoparticles are observed in the $Cu_{0.75}Fe_{0.25}$ sample and the contact between some of the Cu and Fe nanoparticles is confirmed. When increasing the content of Fe, the contact between Cu and Fe nanoparticles increases accordingly, as can be seen in the $Cu_{0.50}Fe_{0.50}$@C (see **Figure S40**) and $Cu_{0.24}Fe_{0.76}$@C (see **Figure S41**) sample. When the content of Fe in the bimetallic CuFe samples continue to increase, large agglomerates of Fe nanoparticles with very few Cu surrounding can be seen in the $Cu_{0.12}Fe_{0.88}$@C and $Cu_{0.08}Fe_{0.92}$@C sample (as shown in **Figure S42** and **Figure S43**), suggesting the lower possibility to form contact between Cu and Fe nanoparticles in these two samples.

According to the morphological characterizations and the physiochemical properties of CuFe alloy structures, we can have a general idea on the chemical composition and spatial distributions of Cu and Fe in the CuFe@C NPs prepared in this work. As depicted in **Figure 5**, four types of NPs can co-exist in the bimetallic CuFe samples, including monometallic Cu and Fe NPs and bimetallic Fe-dominant and Cu-dominant NPs. For simplification, we use core-shell structure to describe those CuFe bimetallic nanoparticles to show the formation of interfacial contact between Cu and Fe domains. According to the EDS mapping results from both FESEM and STEM, monometallic Cu NPs and Cu-dominant bimetallic NPs contribute the majority in the $Cu_{0.75}Fe_{0.25}$@C sample. When increasing the Fe content in the sample to form $Cu_{0.24}Fe_{0.76}$@C sample, a much higher amount of Fe-dominant bimetallic nanoparticles will be formed. However, when the Cu content is very low in the bimetallic CuFe samples (such as the $Cu_{0.08}Fe_{0.92}$@C sample), then monometallic Fe NPs as well as a small fraction of Fe-dominant bimetallic NPs will be the most abundant species (see **Figure 5**).

Catalytic studies with CuFe bimetallic nanoparticles

Herein, the chemoselective hydrogenation of 5-(hydroxymethyl)furfural (HMF) to 2,5-bis(hydroxymethyl)furan (BHMF) was chosen to study how the chemical composition of CuFe bimetallic nanoparticles influence their catalytic behavior. Firstly, we have measured the monometallic nanoparticles under mild conditions (110 ºC with 10 bar of H_2). As can be seen in **Figure 6**, Fe@C NPs showed a very low yield of BHMF after reaction for 6 h and only 25% conversion of HMF as well as 21% yield of BHMF was obtained after 24 h reaction. As shown before in **Figure 2b**, a very low initial reaction rate and long induction period can be observed when using Fe@C NPs as the catalyst, which should be related to the reduction of surface FeOx patches under reaction conditions. When a small amount of Cu (~8% atomic ratio respect to the total amount of metal) was introduced to Fe@C NPs during the synthesis to form the $Cu_{0.08}Fe_{0.92}$@C sample, a clear improvement in the activity was observed, especially at the starting stage (see **Figure S44**). A further increase of activity can be obtained with the $Cu_{0.12}Fe_{0.88}$@C sample, leading to a higher yield of BHMF than the corresponding monometallic components. The $Cu_{0.24}Fe_{0.76}$@C sample, with more Cu on Fe nanoparticles, exhibits both high activity (94% conversion of HMF at 4 h) and high chemoselectivity (~100% to BHMF). By looking into the kinetic curves (see **Figure S45** to **Figure S48**), the induction period also becomes shorter when the activity of the CuFe catalyst goes higher. Interestingly, if the amount of Cu in the

bimetallic CuFe catalyst is further increased, the activity starts to drop since the population of the Fe nanoparticles with Cu on the surface decreases (see **Figure 5**). In terms of the $Cu_{0.50}Fe_{0.50}$@C and $Cu_{0.75}Fe_{0.25}$@C samples, similar initial reaction rates were obtained as the $Cu_{0.08}Fe_{0.92}$@C and $Cu_{0.12}Fe_{0.88}$@C samples, give much lower yield of BHMF than the best-performing $Cu_{0.24}Fe_{0.76}$@C sample (see **Figure 6b**). The dramatic difference between various CuFe catalysts suggests the strong correlation between the hydrogenation reactivity and catalyst structure.

It should be noted that, for all the non-noble metal nanoparticles, high selectivity to BHMF (~100% selectivity at >90% conversion) can be obtained, reinforcing the advantages of using non-noble metal catalysts as substitutes for noble metal catalysts.

Taking into account that Fe@C gives negligible activity in the first 6 h during hydrogenation of HMF, we have attempted to normalize the initial reactivity of Cu-containing catalysts to the Cu mass. As can be seen in **Figure 6c**, the $Cu_{0.24}Fe_{0.76}$@C sample still delivers the best performance. Nevertheless, we have compared the catalytic performance of the $Cu_{0.24}Fe_{0.76}$@C sample with non-noble metal catalysts reported in recent literature for hydrogenation of HMF to BHMF. As summarized in **Table S2**, the bimetallic CuFe@C catalyst presented here gives higher activity per gram of catalysts than Cu and Ni-based catalysts.

The monometallic Cu@C sample gives moderate activity for hydrogenation of HMF to BHMF, and its initial reactivity is apparently better than $Cu_{0.50}Fe_{0.50}$ and $Cu_{0.75}Fe_{0.25}$ samples (see **Figure S49**). According to the structural characterization results obtained by electron microscopy, the introduction of Fe may cause the formation of FeOx patches on the surface of metallic Cu nanoparticles. For comparison, we have prepared a Fe/Cu@C sample by impregnating ~25 wt% of Fe on Cu@C nanoparticles. As can be seen in **Figure S50**, the Fe/Cu@C sample show even lower activity than Cu@C nanoparticles, indicating the presence of Fe species on the surface of Cu@C may block the active sites in Cu@C nanoparticles.

We have also tested the physical mixture of Fe@C and Cu@C nanoparticles with a molar ratio of 3:1 to compare with the best-performing $Cu_{0.24}Fe_{0.76}$@C sample under the same reaction conditions. As shown in **Figure S51**, the physical mixture shows much lower activity than the bimetallic $Cu_{0.24}Fe_{0.76}$@C sample, implying that the active sites in the $Cu_{0.24}Fe_{0.76}$@C sample should be related to the intimate contact between the two elements (Cu and Fe).

We have studied the detailed spatial distributions of Cu species on Fe nanoparticles by STEM-EDS mapping. As can be seen in **Figure 7** and **Figure S52-S54**, both Cu nanoparticles (ranging from several nanometer to tens of nanometer) on the external surface and highly dispersed Cu species (atomically or subnanometric Cu clusters) on the surface or doped on the Fe nanoparticles can be found in the Fe matrix, as illustrated in **Figure 8**. The CuFe@C samples ($Cu_{0.50}Fe_{0.50}$@C and $Cu_{0.75}Fe_{0.25}$@C) with higher Cu loadings and abundance of large Cu nanoparticles show lower activity than the $Cu_{0.24}Fe_{0.76}$@C sample, indicating the large Cu nanoparticles should not be the most active species for hydrogenation of HMF. Moreover, the amount of Cu species doped in the Fe matrix should be very low (<1 wt.%) due to the immiscible nature of the two elements. In addition, we have also observed those highly dispersed Cu species doped in Fe nanoparticles in the less active samples ($Cu_{0.12}Fe_{0.88}$@C and $Cu_{0.08}Fe_{0.92}$@C). Combining the results shown in **Figure 2** and **Figure 6c**, in which the catalysts with a better dispersion of Cu species show much higher specific activities normalized to the Cu mass, we speculate that the small Cu nanoparticles dispersed on Fe nanoparticles are the key active sites for hydrogenation of HMF. The size distribution of Cu species among various CuFe@C samples are different and dependent on the Cu/Fe ratio used in the synthesis, resulting in the composition-dependent catalytic performance observed among the bimetallic CuFe@C catalysts.

The above morphological characterizations have shown how the distributions of Cu and Fe in the bimetallic CuFe@C samples vary with the Cu/Fe ratio. The surface properties have also been studied by X-ray photoelectron spectroscopy (XPS), and as shown in **Figure 9a-b**, the surface Fe species are in oxidized state in both Fe@C and $Cu_{0.24}Fe_{0.76}$@C, as was previously observed by electron microscopy.

After in situ reduction treatment at 110 °C with H_2, partial reduction (9.8%) of FeOx (mixture of Fe(II) and Fe(III)) into metallic Fe(0) can be observed in Fe $2p_{3/2}$ region. Notably, the percentage of metallic Fe formed in $Cu_{0.24}Fe_{0.76}$@C sample is higher than in the reduced Fe@C sample (28.3% vs. 9.8%), indicating a clear promotion effect of Cu for reduction of FeOx species. Considering the promotion effect of Cu on reduction of FeOx may occur through H spillover mechanism, the metallic Fe formed in the reduced $Cu_{0.24}Fe_{0.76}$@C sample may be physically close to the Cu nanoparticles.[50, 51] This is supported by the shift in the binding energy (BE) of the Fe^0 species in the $Cu_{0.24}Fe_{0.76}$@C sample

(located at 708.1 eV) versus Fe@C (at 707.0 eV) (**see Table S3**), in accordance with the higher electronegativity of Cu versus Fe. In terms of the Cu species, a reduction of Cu(II) into Cu(I) and Cu(0) in the pristine $Cu_{0.24}Fe_{0.76}$@C sample has also been observed in the Cu $2p_{3/2}$ region (see **Figure 9c**) since the shake-up peak associated with Cu(II) decreases significantly after reduction treatment. Transformation of Cu(I) into metallic Cu(0) is also confirmed by the Auger spectra (see **Figure 9d**). These results indicate that, both metallic Cu(0) and Fe(0) are present in the $Cu_{0.24}Fe_{0.76}$@C sample under the reaction conditions for hydrogenation of HMF and Cu facilitates the reduction of FeOx in the presence of hydrogen. This is supported by the temperature-programmed reduction data (Figure S55). After this, both metallic Cu and surface metallic Fe formed by reduction of surface FeOx should be able to activate hydrogen. If this is so, then, the composition-dependent catalytic behavior of bimetallic CuFe@C catalysts could be correlated in our case with their by ability for H_2 activation that we could measure by means of H_2-D_2 exchange experiments. Then, as presented in **Figure 10**, the monometallic Fe@C sample shows poor activity for H_2-D_2 exchange, which corresponds to its very low activity in the hydrogenation reaction. The $Cu_{0.24}Fe_{0.76}$@C sample shows the highest activity among the bimetallic CuFe@C samples for the production of HD in the isotopic studies, being consistent with the highest content of Cu and Fe reduced species and the catalytic activity for hydrogenation of HMF. As we discussed before, it is speculated that small Cu particles (probably 2-10 nm according to the EDS mapping in **Figure 7**) supported on Fe nanoparticles are the plausible most active species for the hydrogenation of HMF. Those small Cu particles give higher activity for isotopic H_2-D_2 exchange than atomically dispersed Cu species in the Fe matrix, which is consistent with our recent observation with supported Pt catalysts, in which small Pt clusters and nanoparticles (~1 nm) show higher reactivity for H_2-D_2 exchange and hydrogenation reactions than isolated Pt atoms and larger nanoparticles (>2 nm).[52] Moreover, metallic Fe sites are also formed in the $Cu_{0.24}Fe_{0.76}$@C sample due to the Cu-promoted reduction of the surface FeOx patches and those metallic Fe sites can also be active for H_2 activation. The contribution from both exposed metallic Cu and Fe sites account for the higher activity of $Cu_{0.24}Fe_{0.76}$@C than Cu@C for the isotopic H-D exchange and hydrogenation of HMF

In conclusion, we propose a plausible catalyst model, as described in **Figure 11** to explain the high

catalytic activity observed with the $Cu_{0.24}Fe_{0.76}$@C sample nanoparticles for hydrogenation of HMF to BHMF. In the fresh catalyst, the surface of pure Fe nanoparticles is almost completely covered by FeOx patches. It has been reported in the literature, Fe@C nanoparticles obtained by reduction of Fe-EDTA precursor can give high conversion (>99%) and good selectivity (~83%) in hydrogenation of furfural to furfuryl alcohol at high temperature (220 ºC).[53] It can be expected that, a much higher percentage of FeOx can be reduced under such a high reaction temperature. However, under the mild conditions used in this present work, in the case of bimetallic $Cu_{0.24}Fe_{0.76}$@C sample, surface FeOx patches can be partially reduced to metallic Fe under the promotion effect from small Cu nanoparticles. Thus, the exposed surface metallic sites are largely increased compared to the Fe@C sample, leading to an enhancement for H_2 activation and for hydrogenation of HMF to BHMF. If comparing the catalytic performance of $Cu_{0.24}Fe_{0.76}$@C sample to the highly reduced Fe@C catalyst in the literature, the bimetallic $Cu_{0.24}Fe_{0.76}$@C sample gives similar reaction for hydrogenation of C=O group though it works at a much lower temperature (110 vs. 220 ºC).

Interestingly, when comparing the performance of the $Cu_{0.24}Fe_{0.76}$@C catalyst with those based on noble metals reported in literature for the hydrogenation of HMF into BHMF (**Table S4**), it can be seen that the selectivity to BHMF obtained with CuFe@C catalyst is similar to the exhibited by the noble metals catalysts.

Stability tests on CuFe@C catalyst

The heterogenous nature of the HMF hydrogenation reaction by CuFe@C nanoparticles was confirmed by the hot filtration experiment. After removing the solid catalyst, the hydrogenation reaction was paused (see **Figure S56**). Finally, the stability of $Cu_{0.24}Fe_{0.76}$@C sample has been tested by consecutive recycling tests. As can be seen in **Figure S57**, after four catalytic runs, only a slight deactivation has been observed. Since the recycled catalyst was only washed with acetone, some reactions or products may be absorbed on the surface of the bimetallic CuFe nanoparticles, resulting in the slight deactivation. Nevertheless, these results clearly demonstrate the much higher stability of bimetallic CuFe nanoparticles encapsulated in thin carbon layers than the Cu nanoparticles generated on solid carriers by conventional impregnation method. The morphology of $Cu_{0.24}Fe_{0.76}$@C sample after four consecutive catalytic cycles is preserved and the small Cu particles dispersed on Fe nanoparticles can

be identified in the EDS mapping images (see **Figure S58 to S63**).

Experimental Section

Materials synthesis

As supports we have used here: TiO_2 (nanopowder, supplied by Merck, product code: 718467-100G), Fe_2O_3 (nanopowder, supplied by Merck, product code: 544884-25G), ZrO_2 (nanopowder, supplied by Merck, product code: 544760-25G) and Al_2O_3 (nanopowder, supplied by NanoActive^{TM}). Supported Cu catalysts on the different solid carriers (TiO_2, Al_2O_3, Fe_2O_3 and ZrO_2) were firstly prepared by conventional wetness impregnation. Then, a portion of $Cu(NO_3)_2$ solution was mixed with the solid carrier and kept stirring for 2 h at room temperature. Excess water was removed by heating at 120 ºC and the resultant solid product was dried in an electric oven at 60 ºC overnight. The supported Cu catalysts were obtained after reducing the above solid products by H_2 at 300 ºC.

In another procedure, CuFe-EDTA complexes with different Cu/Fe ratios were prepared by hydrothermal reaction of the Cu and Fe nitrate salts with sodium EDTA solution. The experimental details for the preparation of non-noble metal nanoparticles with various chemical compositions are summarized in **Table S1**. The resultant solution was placed in autoclave for hydrothermal reaction at 200 ºC for 24 h. After the hydrothermal reaction, the solid product (CuFe-EDTA complex) was isolated by filtration and then washed with water and acetone. Then, CuFe bimetallic nanoparticles were obtained by reduction of the CuFe-EDTA complexes with H_2 at 450 ºC. After being reduced at 450 ºC for 4 h, the sample was cooled to room temperature in H_2 flow and then kept in glass vial. For monometallic Cu and Fe nanoparticles, they were prepared in the same way but using only Cu nitrate or Fe nitrate as the metal precursor.

Characterizations

Powder X-ray diffraction (XRD) was performed with a HTPhilips X'Pert MPD diffractometer equipped with a PW3050 goniometer using Cu Kα radiation and a multisampling handler.

Samples for electron microscopy studies were prepared by dropping the suspension of solid sample using CH_2Cl_2 as the solvent directly onto holey-carbon coated copper grids. All the measurements

were performed in a JEOL 2100F microscope operating at 200 kV both in transmission (TEM) and scanning-transmission modes (STEM). STEM images were obtained using a High Angle Annular Dark Field detector (HAADF), which allows Z-contrast imaging.

X-ray photoelectron spectroscopy (XPS) measurements were performed on a SPECS spectrometer with a MCD-9 detector and using a non monochromatic MgKα (1253.6 eV) X-Ray source. Spectra were recorded using analyzer pass energy of 30 eV, an X-ray power of 100W and under an operating pressure of 10^{-9} mbar. Spectra treatment has been performed using the CASA software. Binding energies (BE) were referenced to C1s at 284.5 eV.

The redox properties of catalysts were evaluated by Temperature-programmed reduction (TPR). Micrometrics Autochem 2910 catalyst characterization system with a thermal conductivity detector (TCD) was used. Prior to TPR analysis, about 40 mg of the catalyst was pretreated at room temperature in flowing argon for 30 min. The argon gas was switched to 10% H_2 in argon with a flow rate of 50 mL min-1 and the temperature was increased to 750 ºC at a ramping rate of 10 ºC min-1.

H_2-D_2 exchange experiments were carried out in a flow reactor. The feed gas consisted of 4 mL/min H_2, 4 mL/min D_2 and 18 mL/min argon, and the total weight of catalyst was ca. 100 mg. Reaction products (H_2, HD and D_2) were analysed with a mass spectrometer (Omnistar, Balzers). For the samples that need to be reduced before the H_2-D_2 exchange experiments, they were *in situ* reduced at 110 ºC for 2 h with a temperature-rising rate of 10 ºC/min.

Catalytic studies

The chemoselective hydrogenation of HMF to BHMF was performed in batch reactors. 0.5 mmol of HMF, internal standard (dodecane), solvent (5 mL of methanol), 10 mg powder catalyst and a magnetic bar was added. After the reactor was sealed, air was purged by flushing twice with 10 bar of hydrogen. Then the autoclave was pressurized with H_2 to the corresponding pressure. The stirring speed is kept at 900 rpm and the size of the catalyst powder is below 0.05 mm to avoid either external or internal diffusion limitations. Finally, the batch reactor was heated to the target temperature. The products were also analyzed by GC and GC-MS. The stability of CuFe@C catalysts has been tested by isolating the used catalyst from the reaction mixture, washing with acetone and reusing in a consecutive catalytic test.

Conclusions

In this work, we have shown the synthesis and structural characterization of bimetallic CuFe@C nanoparticles. By varying the Cu/Fe ratio, the spatial distribution of Cu and Fe in the bimetallic sample can be tuned and has a clear influence on catalytic performance for chemoselective hydrogenation of HMF to BHMF. The optimized $Cu_{0.24}Fe_{0.76}$@C sample shows excellent activity and selectivity, which could be related to the formation of small metallic Cu nanoparticles on the surface of the Fe particles and which promote the reduction of the FeOx formed on the external layers of the Fe nanoparticles at lower temperatures with hydrogen. Our results indicate that, by the combination of two less active non-noble metals, it is possible to prepare a highly active and selective hydrogenation catalyst by tuning the particle size, chemical composition and spatial distribution of the two metal components.

Conflicts of interest

There are no conflicts to declare.

Acknowledgement

This work has been supported by the Spanish government through the "Severo Ochoa Program" (SEV-2016-0683) and the PGC2018-097277-B-100 (MCIU/AEI/FEDER, UE) project. The authors also thank Microscopy Service of UPV for the TEM and STEM measurements. A.G.-O. thanks Severo Ochoa Program for predoctoral fellowships.

Keywords: CuFe nanoparticles, biomass valorization, 5-(hydroxymethyl) furfural, 2,5-bis(hydroxymethyl)furan, chemoselective hydrogenation

REFERENCES

1. J. J. Bozell and G. R. Petersen, *Green Chemistry*, 2010, **12**, 539-554.
2. M. J. Climent, A. Corma and S. Iborra, *Green Chemistry*, 2014, **16**, 516-547.
3. A. Corma, S. Iborra and A. Velty, *Chemical Reviews*, 2007, **107**, 2411-2502.

4. R.-J. van Putten, J. C. van der Waal, E. de Jong, C. B. Rasrendra, H. J. Heeres and J. G. de Vries, *Chemical Reviews*, 2013, **113**, 1499-1597.
5. L. Liu, P. Concepción and A. Corma, *Journal of Catalysis*, 2016, **340**, 1-9.
6. L. Cottier, G. Descotes and Y. Soro, *Synthetic Communications*, 2003, **33**, 4285-4295.
7. A. Gelmini, S. Albonetti, F. Cavani, C. Cesari, A. Lolli, V. Zanotti and R. Mazzoni, *Applied Catalysis B: Environmental*, 2016, **180**, 38-43.
8. L. Hu, L. Lin and S. Liu, *Industrial & Engineering Chemistry Research*, 2014, **53**, 9969-9978.
9. M. Besson, P. Gallezot and C. Pinel, *Chemical Reviews*, 2014, **114**, 1827-1870.
10. G. W. Huber, S. Iborra and A. Corma, *Chemical Reviews*, 2006, **106**, 4044-4098.
11. Z.-L. Wu, J. Wang, S. Wang, Y.-X. Zhang, G.-Y. Bai, L. Ricardez-Sandoval, G.-C. Wang and B. Zhao, *Green Chemistry*, 2020, **22**, 1432-1442.
12. K. Wang, W. Zhao, Q. Zhang, H. Li and F. Zhang, *ACS Omega*, 2020, **5**, 16183-16188.
13. J. Tan, J. Cui, Y. Zhu, X. Cui, Y. Shi, W. Yan and Y. Zhao, *ACS Sustainable Chemistry & Engineering*, 2019, **7**, 10670-10678.
14. L. E. Sousa AF, Valentini A, Diógenes ICN., *J. Braz. Chem. Soc.*, 2020, **31(7)**, 1362-1369.
15. M. B. Modelska, M.J.; Kaminski, Z.; Karski, S.; Kolesinska, B.; Mierczynski, P.; Severino, C.J.; Stanishevsky, A.; Witonska, I.A., *Catalysts*, 2020, **10**, 444.
16. B. Ledesma, J. Juárez, J. Mazarío, M. Domine and A. Beltramone, *Catalysis Today*, 2021, **360**, 147-156.
17. M. Balakrishnan, E. R. Sacia and A. T. Bell, *Green Chemistry*, 2012, **14**, 1626-1634.
18. H. Cai, C. Li, A. Wang and T. Zhang, *Catalysis Today*, 2014, **234**, 59-65.
19. J. Han, Y.-H. Kim, B. Y. Jung, S. H. Hwang, J. Jegal, J. W. Kim and Y.-S. Lee, *Synlett*, 2017, **28**, 2299-2302.
20. F. liu, M. Audemar, K. De Oliveira Vigier, J.-M. Clacens, F. De Campo and F. Jérôme, *Green Chemistry*, 2014, **16**, 4110-4114.
21. J. Ohyama, A. Esaki, Y. Yamamoto, S. Arai and A. Satsuma, *RSC Advances*, 2013, **3**, 1033-1036.
22. B. Op de Beeck, M. Dusselier, J. Geboers, J. Holsbeek, E. Morré, S. Oswald, L. Giebeler and B. F. Sels, *Energy & Environmental Science*, 2015, **8**, 230-240.

23. J. Shi, M. Zhang, W. Du, W. Ning and Z. Hou, *Catalysis Science & Technology*, 2015, **5**, 3108-3112.
24. S. K. Singh, *Asian Journal of Organic Chemistry*, 2018, **7**, 1901-1923.
25. F. A. Westerhaus, R. V. Jagadeesh, G. Wienhöfer, M. M. Pohl, J. Radnik, A. E. Surkus, J. Rabeah, K. Junge, H. Junge, M. Nielsen, A. Brückner and M. Beller, *Nat Chem*, 2013, **5**, 537-543.
26. R. V. Jagadeesh, A.-E. Surkus, H. Junge, M.-M. Pohl, J. Radnik, J. Rabeah, H. Huan, V. Schünemann, A. Brückner and M. Beller, *Science*, 2013, **342**, 1073.
27. R. Millán, L. Liu, M. Boronat and A. Corma, *Journal of Catalysis*, 2018, **364**, 19-30.
28. C. Sarkar, S. Pendem, A. Shrotri, D. Q. Dao, P. Pham Thi Mai, T. Nguyen Ngoc, D. R. Chandaka, T. V. Rao, Q. T. Trinh, M. P. Sherburne and J. Mondal, *ACS Appl Mater Interfaces*, 2019, **11**, 11722-11735.
29. L. Liu, F. Gao, P. Concepción and A. Corma, *Journal of Catalysis*, 2017, **350**, 218-225.
30. L. Liu, P. Concepción and A. Corma, *Journal of Catalysis*, 2019, **369**, 312-323.
31. A. Corma, *Angewandte Chemie International Edition*, 2016, **55**, 6112-6113.
32. S. C. Shit, R. Singuru, S. Pollastri, B. Joseph, B. S. Rao, N. Lingaiah and J. Mondal, *Catalysis Science & Technology*, 2018, **8**, 2195-2210.
33. C. Sarkar, P. Koley, I. Shown, J. Lee, Y.-F. Liao, K. An, J. Tardio, L. Nakka, K.-H. Chen and J. Mondal, *ACS Sustainable Chemistry & Engineering*, 2019, **7**, 10349-10362.
34. P. Koley, S. Chandra Shit, B. Joseph, S. Pollastri, Y. M. Sabri, E. L. H. Mayes, L. Nakka, J. Tardio and J. Mondal, *ACS Applied Materials & Interfaces*, 2020, **12**, 21682-21700.
35. O. Kubaschewski, *Springer-Verla: Berlin*, 1982.
36. H. T. Luk, C. Mondelli, S. Mitchell, S. Siol, J. A. Stewart, D. Curulla Ferré and J. Pérez-Ramírez, *ACS Catalysis*, 2018, **8**, 9604-9618.
37. K. Xiao, Z. Bao, X. Qi, X. Wang, L. Zhong, K. Fang, M. Lin and Y. Sun, *Journal of Molecular Catalysis A: Chemical*, 2013, **378**, 319-325.
38. J. Rojas-Nunez, R. I. Gonzalez, E. M. Bringa, S. Allende, P. Sepúlveda, N. Arancibia-Miranda and S. E. Baltazar, *The Journal of Physical Chemistry C*, 2018, **122**, 8528-8534.
39. C. Sarkar, R. Paul, S. Chandra Shit, Q. T. Trinh, P. Koley, B. S. Rao, A. M. Beale, C.-W. Pao,

A. Banerjee and J. Mondal, *ACS Sustainable Chemistry & Engineering*, 2021, **9**, 2136-2151.

40. Q. Wang, J. Feng, L. Zheng, B. Wang, R. Bi, Y. He, H. Liu and D. Li, *ACS Catalysis*, 2020, **10**, 1353-1365.
41. K. Sun, Y. Shao, Q. Li, Q. Liu, W. Wu, Y. Wang, S. Hu, J. Xiang, Q. Liu and X. Hu, *Molecular Catalysis*, 2019, **474**, 110407.
42. K. S. Arias, J. M. Carceller, M. J. Climent, A. Corma and S. Iborra, *ChemSusChem*, 2020, **13**, 1864-1875.
43. L. Liu, A. V. Puga, J. Cored, P. Concepción, V. Pérez-Dieste, H. García and A. Corma, *Applied Catalysis B: Environmental*, 2018, **235**, 186-196.
44. M. Gupta, M. L. Smith and J. J. Spivey, *ACS Catalysis*, 2011, **1**, 641-656.
45. A. M. Hengne and C. V. Rode, *Green Chemistry*, 2012, **14**, 1064-1072.
46. X. Li, H. Wang, P. Sun, S. Zhang and Z. Yao, *Molecular Catalysis*, 2020, **482**, 110698.
47. M. Besson and P. Gallezot, *Catalysis Today*, 2003, **81**, 547-559.
48. J. Lee, D. H. K. Jackson, T. Li, R. E. Winans, J. A. Dumesic, T. F. Kuech and G. W. Huber, *Energy & Environmental Science*, 2014, **7**, 1657-1660.
49. Y. P. Du and J. S. Luterbacher, *Chimia*, 2019, **73**, 698-706.
50. W. Karim, C. Spreafico, A. Kleibert, J. Gobrecht, J. VandeVondele, Y. Ekinci and J. A. van Bokhoven, *Nature*, 2017, **541**, 68-71.
51. H. O. A. Fredriksson, E. M. Larsson Langhammer and J. W. Niemantsverdriet, *The Journal of Physical Chemistry C*, 2015, **119**, 4085-4094.
52. L. Liu, D. M. Meira, R. Arenal, P. Concepcion, A. V. Puga and A. Corma, *ACS Catalysis*, 2019, **9**, 10626-10639.
53. Z. Zhang, X. Tong, H. Zhang and Y. Li, *Green Chemistry*, 2018, **20**, 3092-3100.

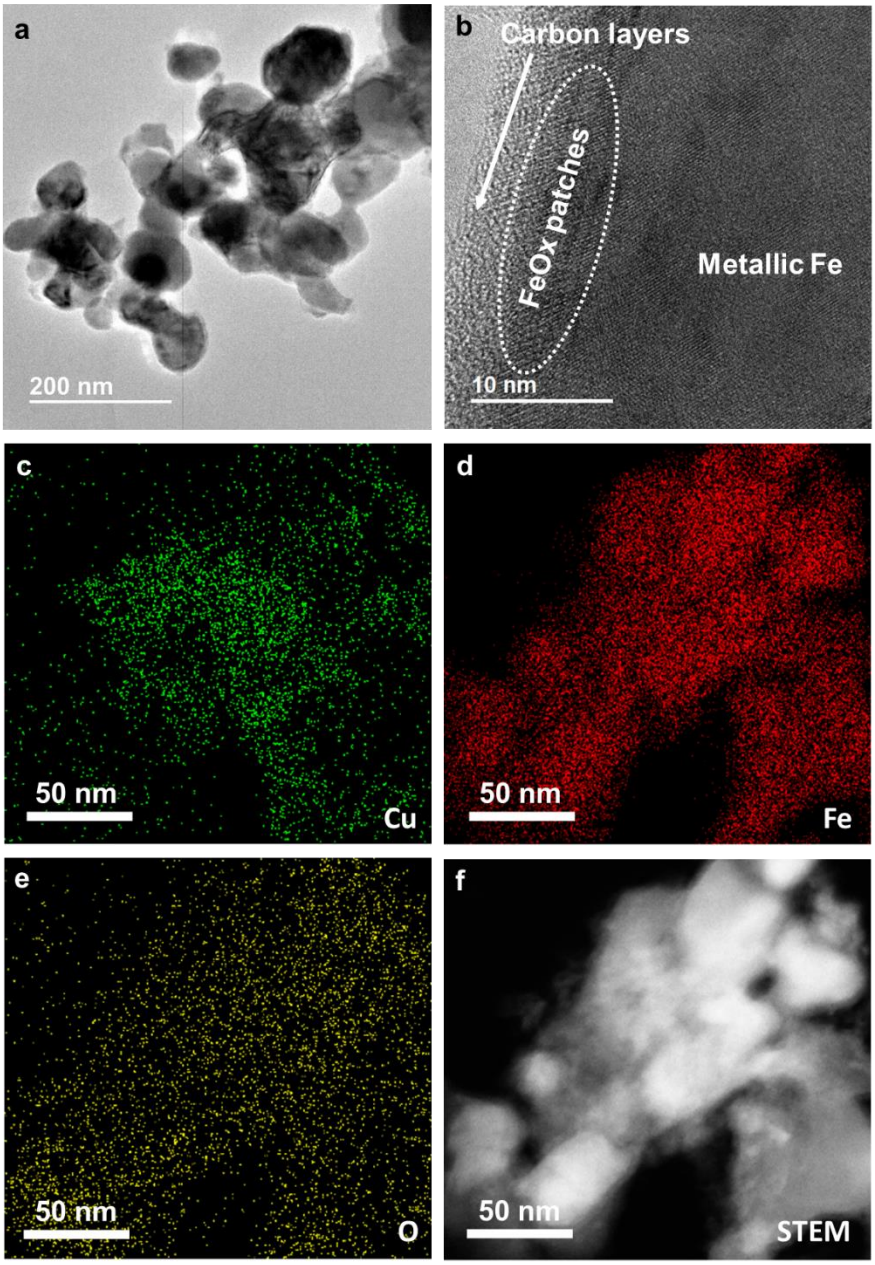

Figure 1. Morphological characterization of Fe@C and 25%Cu/Fe@C sample by electron microscopy. (a, b) TEM images of Fe@C nanoparticles. The Fe nanoparticles are covered by FeOx patches and thin carbon layers. (c-f) STEM image and corresponding X-ray energy dispersion spectroscopy mapping on the distribution of Cu and Fe in the 25%Cu/Fe@C sample. As shown in these images, Cu nanoparticles as well as highly dispersed Cu species on Fe@C nanoparticles can be observed.

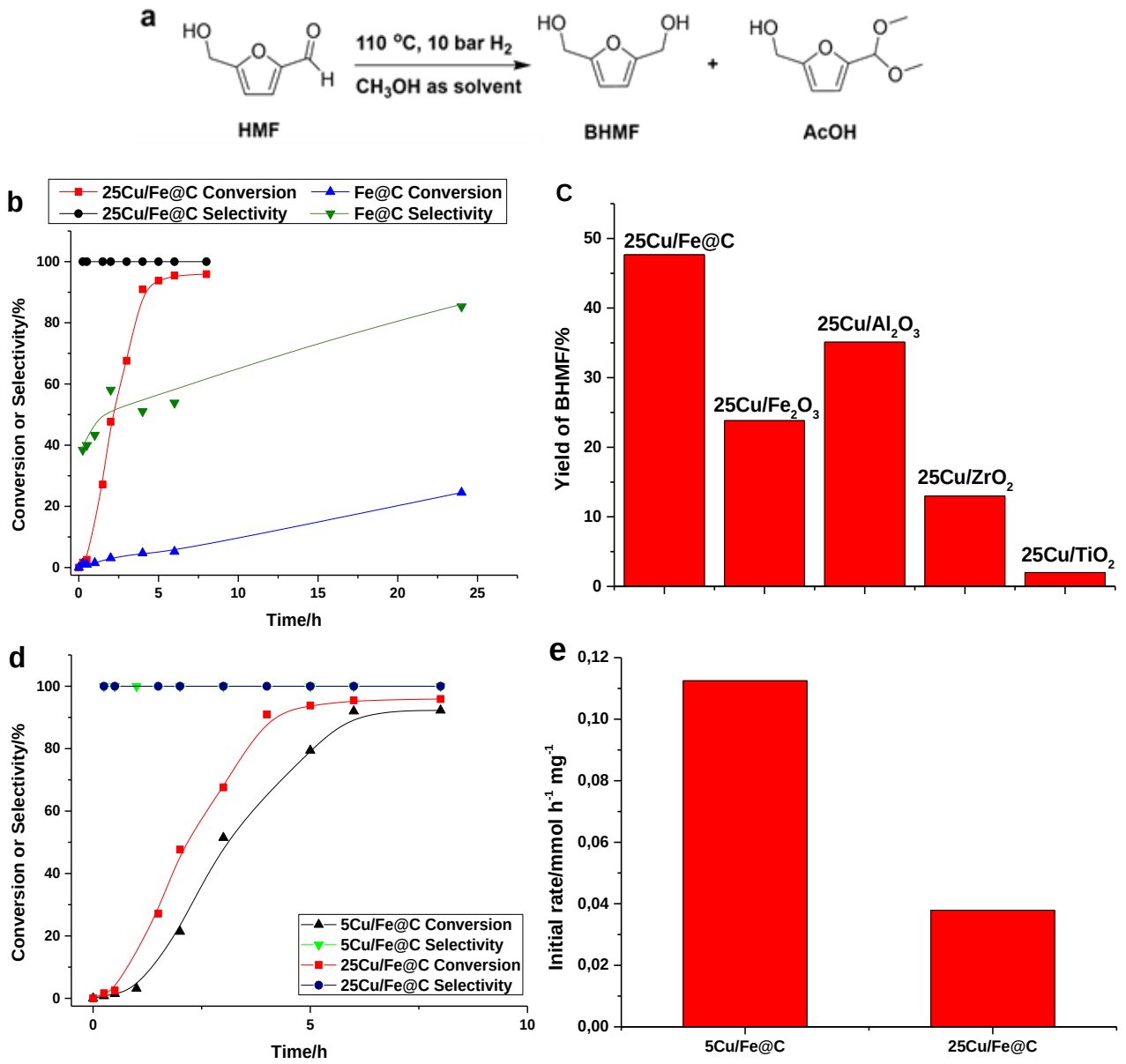

Figure 2. Catalytic performance of different Cu catalysts for hydrogenation of hydrogenation of 5-(hydroxymethyl)furfural (HMF) to 2,5-Bis(hydroxymethyl)furan (BHMF). Acetal (AcOH) is a by-product in this reaction. (a) Reaction scheme and reaction conditions: 10 mg solid catalyst, 0.5 mmol HMF, 5 mL methanol as solvent, 110 °C and 10 bar of H_2. (b) Comparison of Fe@C and Cu/Fe@C with 25 wt% of Cu. (c) Comparison of Cu catalysts on different supports. The yields of BHMF shown in this figure were obtained after reaction for 2 h. (d) Activity of two Cu/Fe@C samples with different Cu loadings tested under the same reaction conditions: 10 mg solid catalyst, 0.5 mmol HMF, 5 mL methanol as solvent, 110 °C and 10 bar of H_2. (e) Initial reaction rates normalized to mass of Cu for hydrogenation of HMF to BHMF.

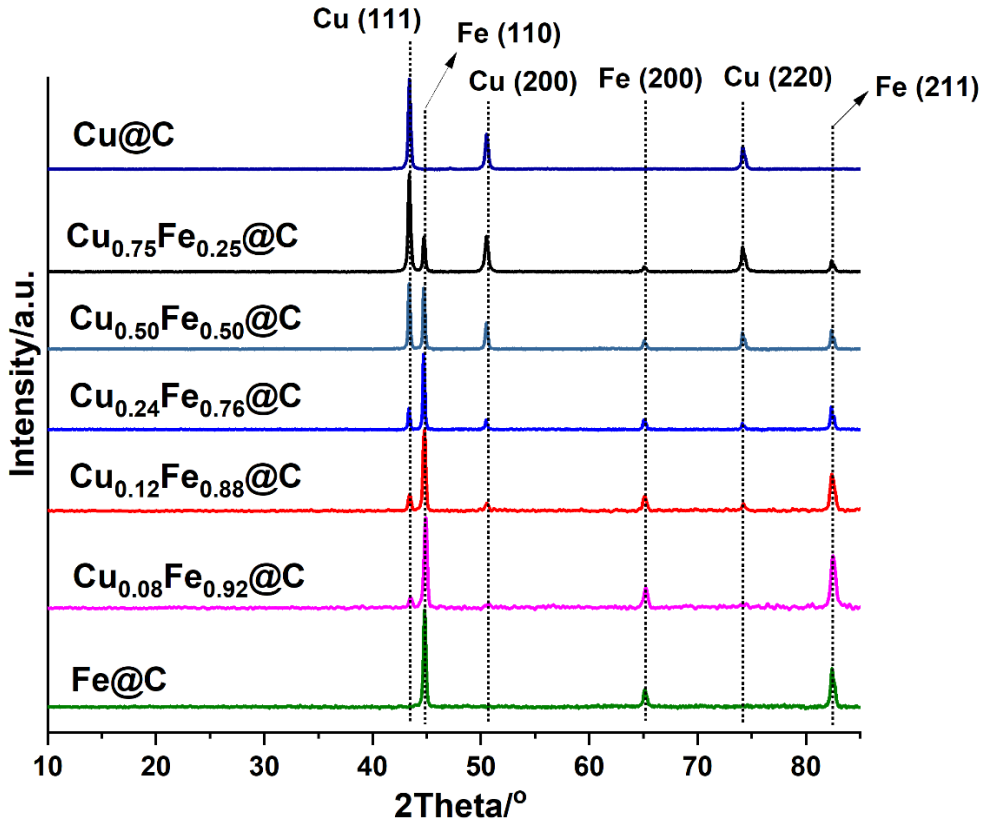

Figure 3. XRD patterns of Cu@C, Fe@C and CuFe@C bimetallic nanoparticles with different chemical compositions. The diffraction peaks have been assigned to the corresponding crystal planes of FCC-type copper and BCC-type iron.

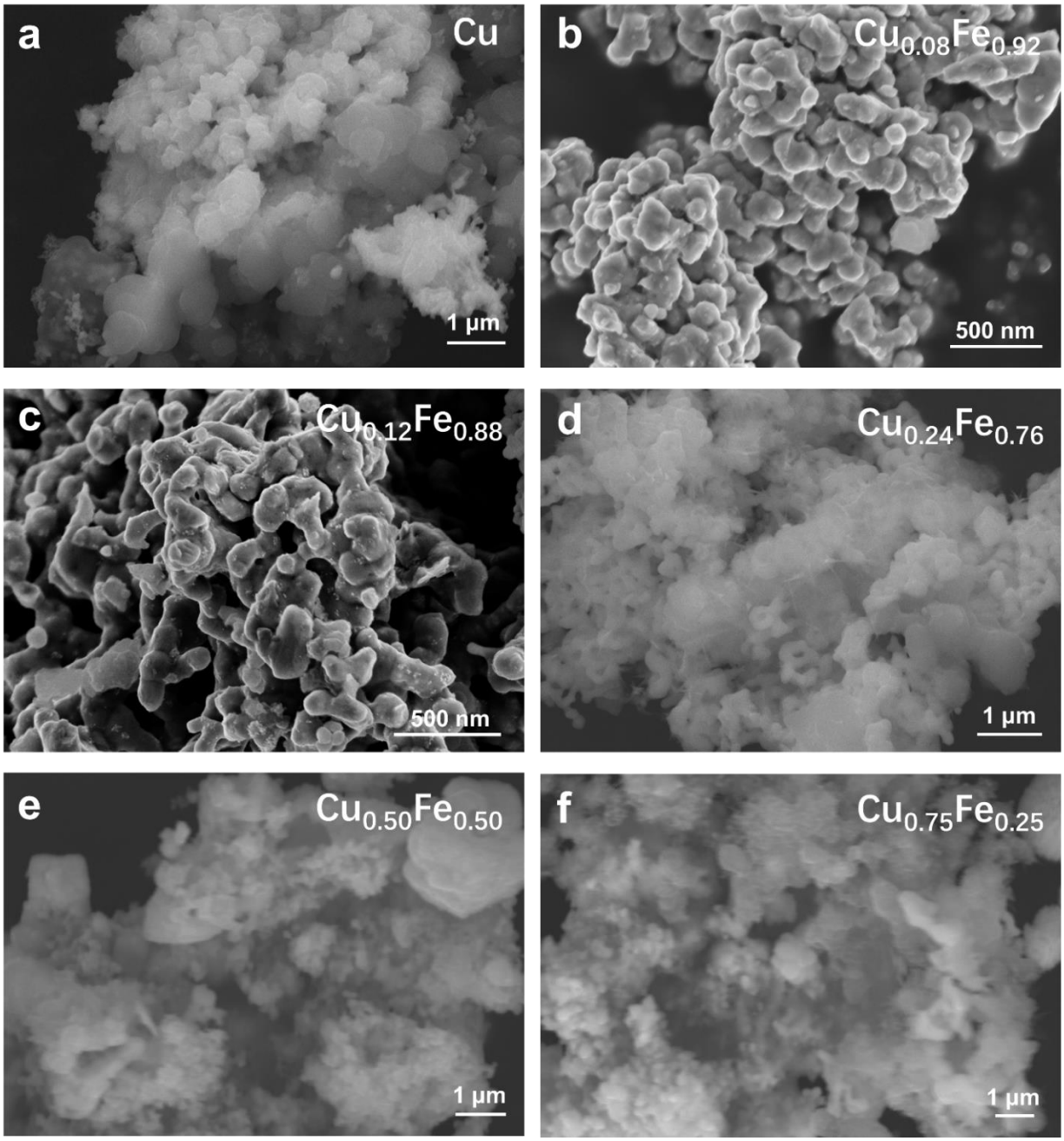

Figure 4. FESEM images of Cu@C and CuFe@C bimetallic nanoparticles with different chemical compositions.

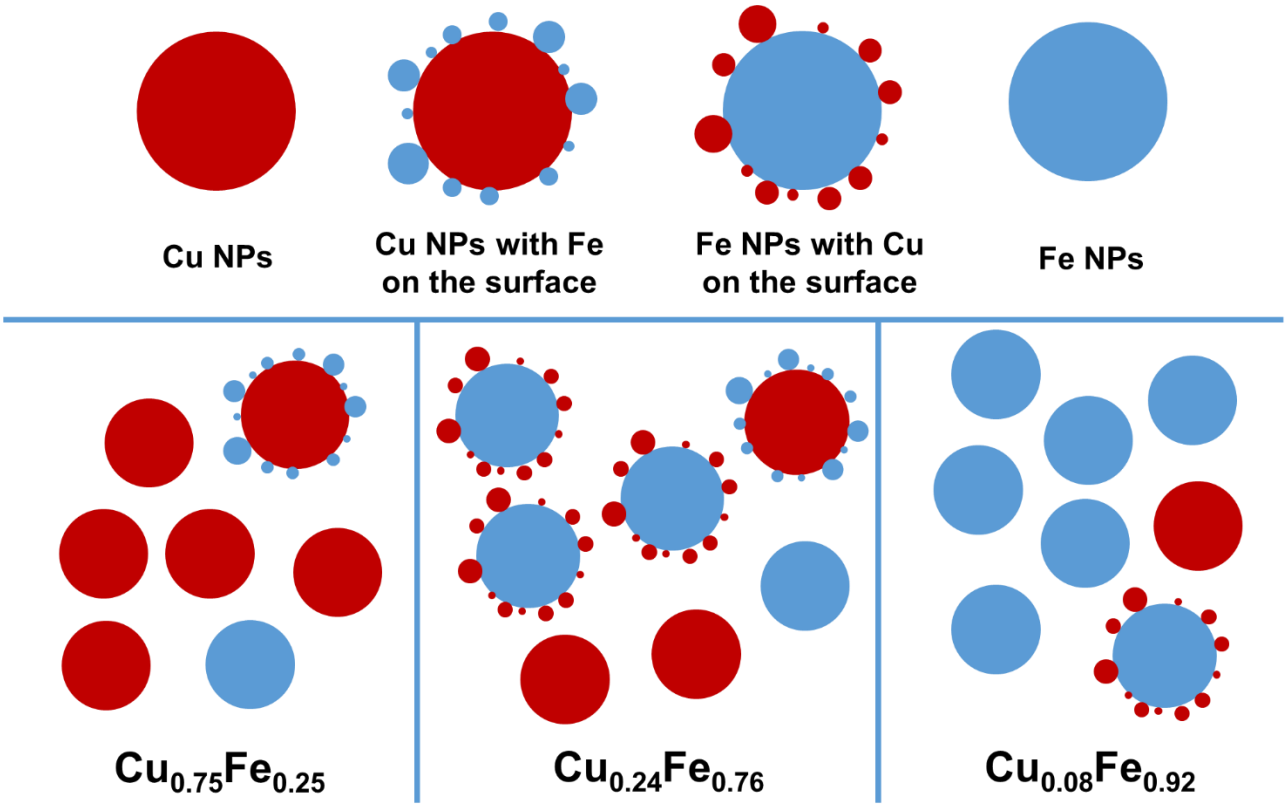

Figure 5. Schematic illustration of the spatial distribution of Cu and Fe elements in the bimetallic

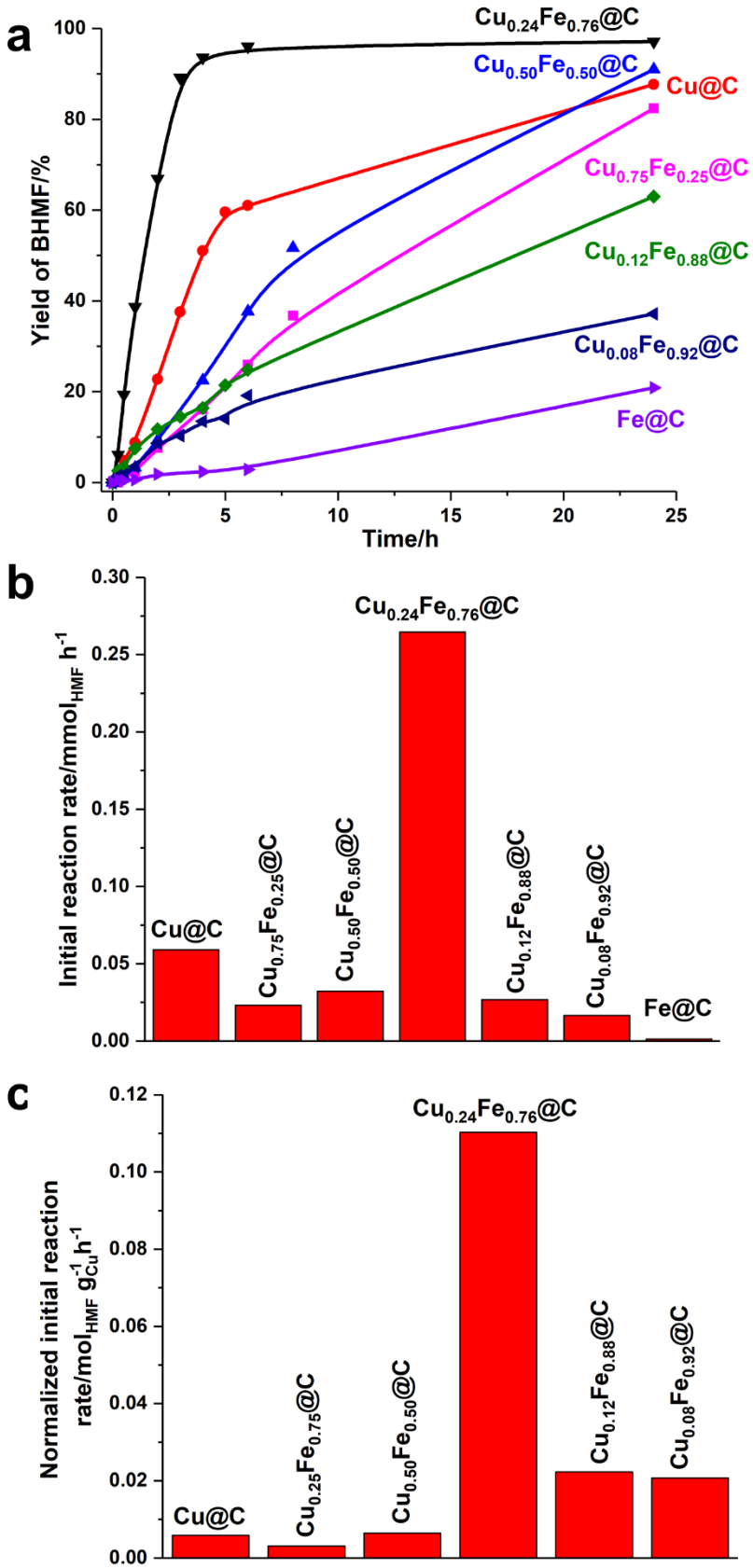

Figure 6. (a) Catalytic performance of Cu@C, Fe@C and bimetallic CuFe@C nanoparticles for hydrogenation of 5-(hydroxymethyl)furfural (HMF) to 2,5-Bis(hydroxymethyl)furan (BHMF).

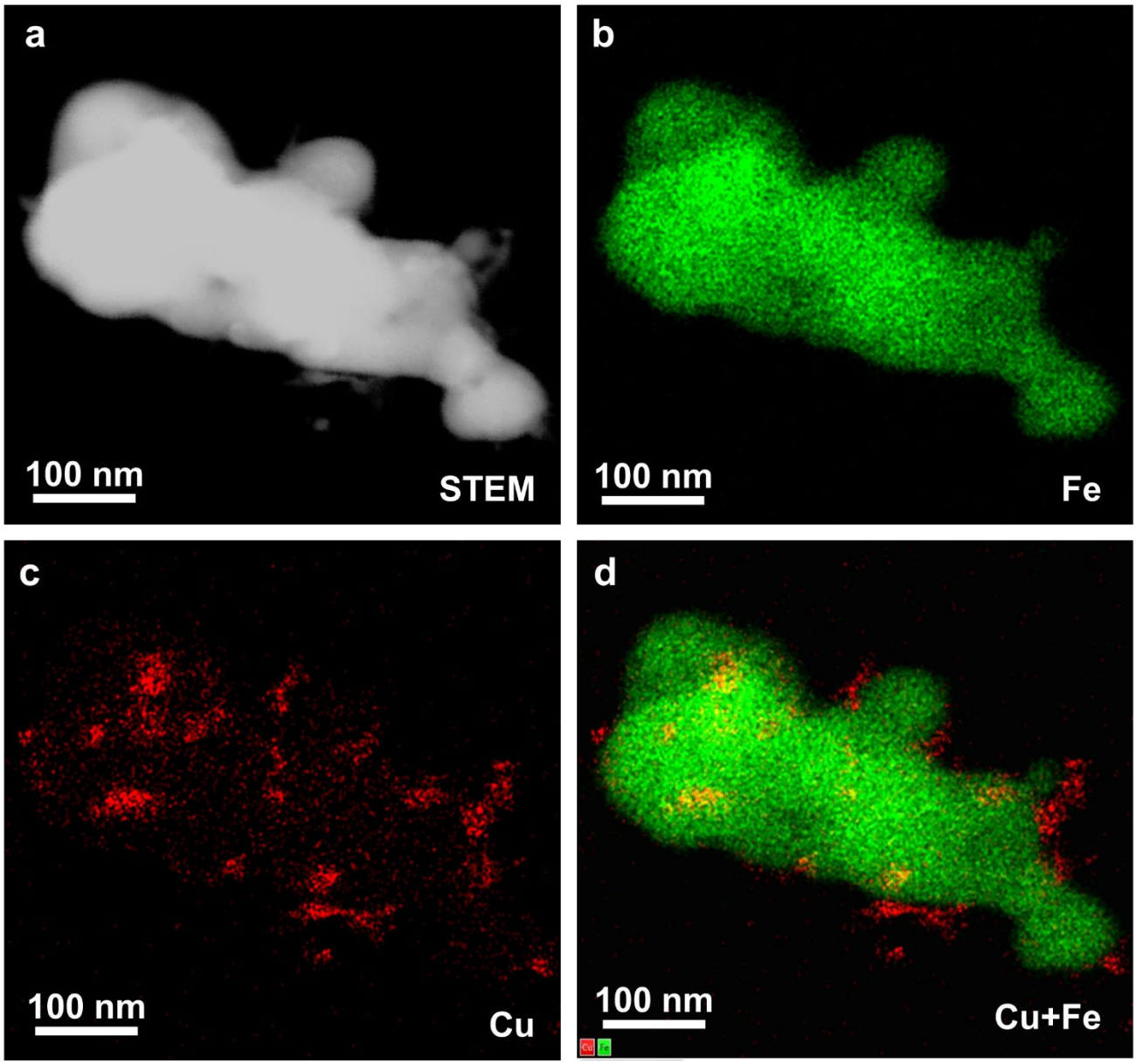

Figure 7. Distributions of Cu species on Fe nanoparticles measured by STEM-EDS mapping in the $Cu_{0.24}Fe_{0.76}$@C sample. As can be seen in (c), Cu patches and highly dispersed Cu species can be observed.

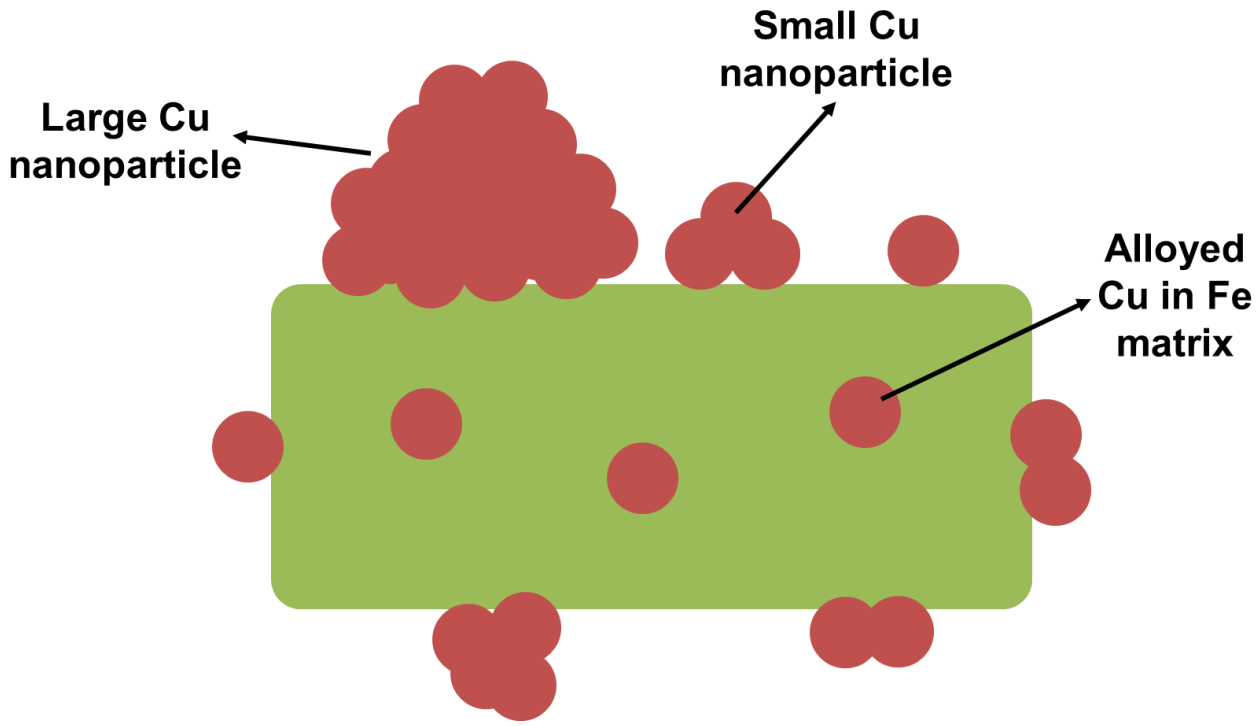

Figure 8. Schematic illustration of different types of Cu species in contact with Fe nanoparticles in the $Cu_{0.24}Fe_{0.76}$@C sample.

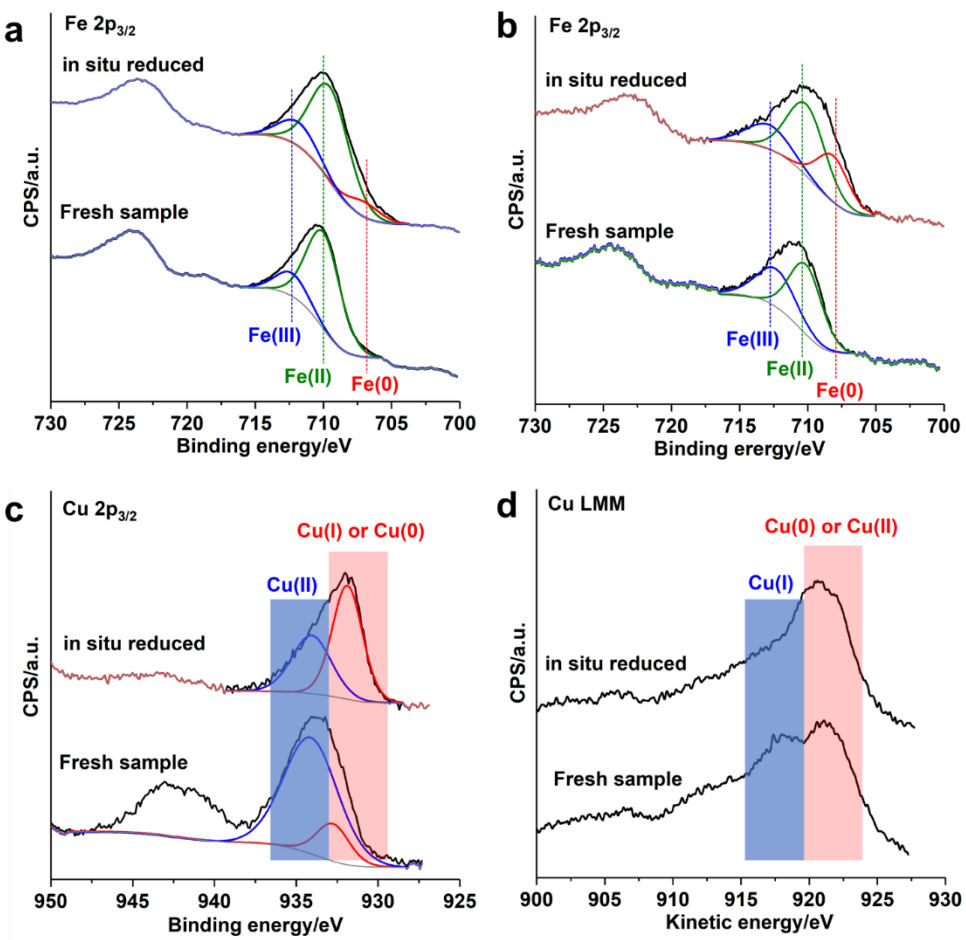

Figure 9. XPS spectra of the fresh Fe@C and $Cu_{0.24}Fe_{0.76}$@C sample and in situ reduced samples. (a) Fe $2p_{3/2}$ region of Fe@C sample, (b) Fe $2p_{3/2}$ region of $Cu_{0.24}Fe_{0.76}$@C sample, (c) Cu $2p_{3/2}$ region of $Cu_{0.24}Fe_{0.76}$@C sample and (d) Cu LMM Auger spectra of $Cu_{0.24}Fe_{0.76}$@C sample. For each sample, both the fresh and in situ reduced (at 110 ºC by H_2 flow) samples were measured.

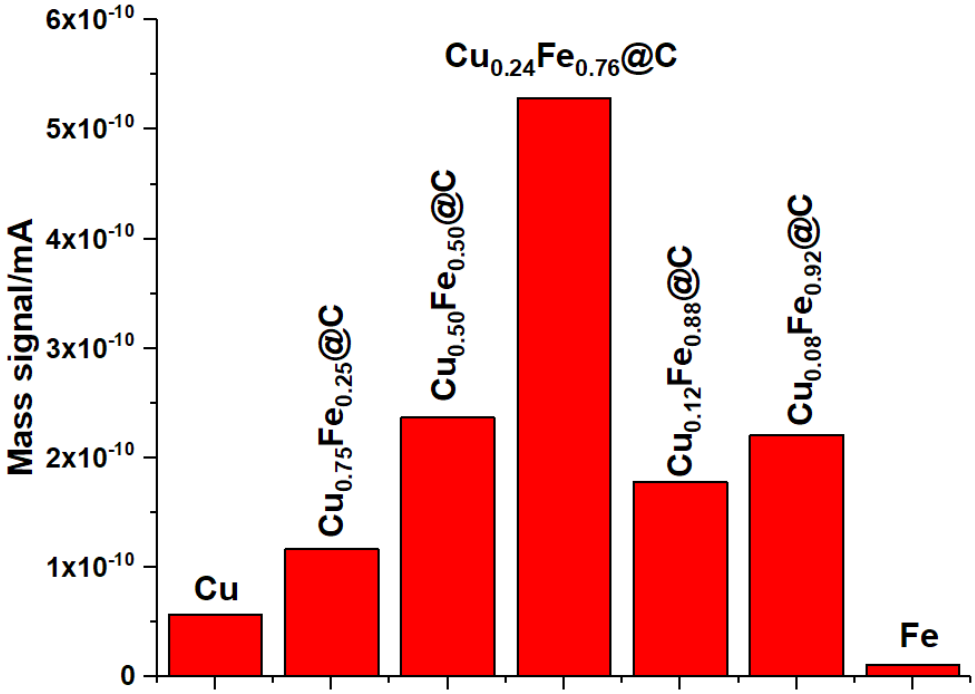

Figure 10. H_2-D_2 exchange on monometallic Cu@C and Fe@C nanoparticles and bimetallic CuFe@C nanoparticles. All the samples were pre-reduced by H_2 at 110 ºC for 2 h before the H_2-D_2 exchange experiments.

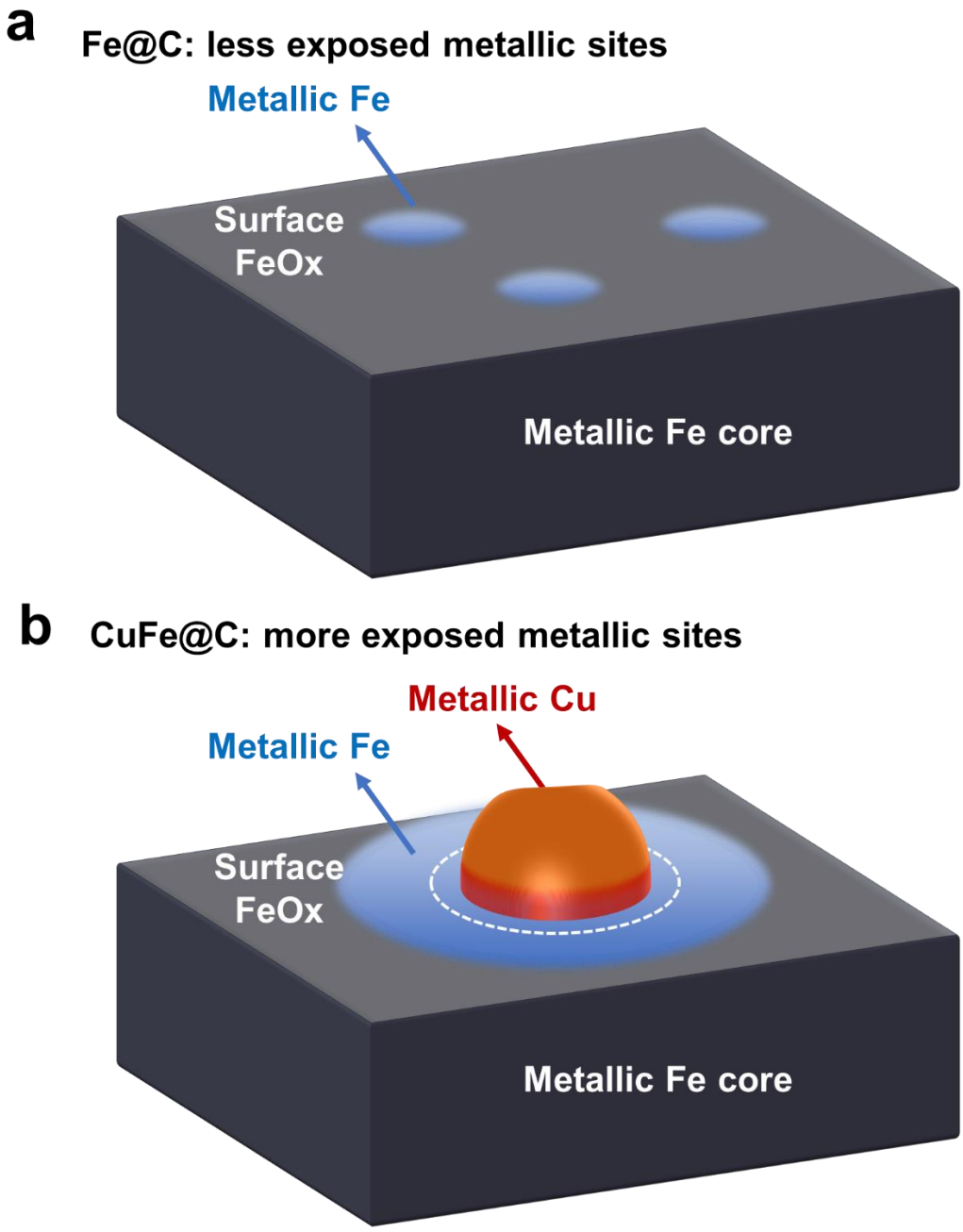

Figure 11. Illustration of the surface structural features of Fe@C and $Cu_{0.24}Fe_{0.76}$@C sample under the reaction conditions for hydrogenation of HMF to BHMF at 110 ºC. In the case of Fe@C (a), only a small portion of the surface of Fe@C nanoparticles will be reduced to metallic Fe while the vast majority will remain to be FeOx, which are inactive for H_2 activation and hydrogenation of HMF. In the case of $Cu_{0.24}Fe_{0.76}$@C sample, most of the Cu nanoparticles will be reduced to metallic Cu and those metallic Cu can further promote the reduction of FeOx into metallic Fe. Consequently, the number of exposed active sites is greatly improved.